Weld Cracking in Duplex Stainless Steel (Report I)†

– Aspects of Solidification Sequence Revealed by Quenching –

Fukuhisa MATSUDA*, Hiroji NAKAGAWA** and Jong-Bong LEE***

Abstract

Solidification sequence of duplex stainless steel weld metals was investigated by observing the typical solidification modes of commercial stainless steels. Freezing the solidification microstructure of each material were made with liquid-tin quenching during GTA welding.

It was found that liquid-tin quenching has sufficient cooling rate to reveal the dendritic substructure near the solidification front even though weld metal solidifies with primary ferrite. This dendritic substructure was gradually obscured with decreasing the temperature even within the BTR, and liquid droplet was confined at the interdendritic boundary due to the development of the solid bridge which was formed at very high temperature near the solidification front. Moreover, the secondary dendrite arm boundary was apt to be obscured compared with the primary dendrite arm boundary. The characteristic features mentioned above was remarkable in dupex and ferritic stainless steels.

KEY WORDS: (Solidification) (Microstructure) (Quenching) (Austenite) (Ferrite) (Stainless Steels)

1. Introduction

In recent years, the hot cracking in duplex stainless steels has been studied[1-6] with considerable attention. According to the results[1,5] studying the effects of ferrite content, the crack susceptibility was minimum at a ferrite level of 5 to 20%, but increases in less or more ferrite than this optimum ferrite range.

Concerning the reason for the increasing the crack susceptibility in the high ferrite range, T. Suutala et al.[7-9] suggested that the crack susceptibility depends upon solidification mode. That is, weld metals which solidify with primary ferrite and subsequent austenite are less susceptible to the cracking than those which solidify with only austenite or ferrite. On the other hand in the previous report[5], it was shown that the microsegration of minor elements within solidification temperature range is the main reason for the increasing the crack susceptibility. However, it was known that the solidification microstructure is hard to observe in the welds which solidify with primary ferrite, due to the postsolidification $\delta \rightarrow \gamma$ phase transformation and the rapid homogenization of microsegregation[10]. Therefore, the solidification microstructure should be revealed clearly in order to study the reason of hot cracking intensively under the viewpoint of microstructure and microsegregation during solidification. From this point of view, S. Kou et al.[10] recently reported that the cellular dendrite of ferritic stainless steel can be observed by liquid-tin quenching during welding.

In the present study, solidification sequence of the several kinds of stainless steels which have different solidification mode has been investigated by means of liquid-tin quenching method. Besides, the cooling effect of liquid-tin quenching method was discussed.

2. Materials and Experimental Procedure

2.1 Materials used

The chemical composition of commercial stainless steels, namely SUS310S, 316L, 304L, 329J2L, 430 and 447J1 are listed in **Table 1**. The thicknesses of these base metals are: (i) 1.5 to 3mm in order to get two-dimensional bead by which the solidification phenomena can be easily analyzed. (ii) 12mm to make a comparison with the Trans-Varestraint cracking test results. The thickness of 6mm of base metal was partly used.

Table 2 shows the chemical composition of the deposited metals for duplex austenitic-ferritic stainless steel,

† Received on Nov. 4, 1987

* Professor
** Research Instructor
*** Graduate Student of Osaka University

Transactions of JWRI is published by Welding Research Institute of Osaka University, Ibaraki, Osaka 567, Japan

SUS329J2L. The deposited metals were made of 4 layers by GTA welding on the base metal of SUS304L plate with several kinds of tentative cored wires. The GTA welding conditions were; welding current of 180A, arc voltage of 17V and welding speed of 20mm/min. The ferrite content in the ambient temperature of the deposited metals was varied in the range of about 0 to 100% on experimental purpose. Then, the overlaid plate was machined to the thickness of 12mm. The size of specimen is 70mm in length and 40mm in width with its thickness.

Table 1 Chemical compositions of base metals of commercial stainless steels

Material	Chemical composition (wt.%)										Thickness
	C	Si	Mn	P	S	Cr	Ni	Mo	N	Others	(mm)
SUS310S(A)	0.070	0.80	1.55	0.016	0.005	25.00	20.08	0.10		O:0.006	2.0
SUS310S(B)	0.070	0.61	1.67	0.022	0.001	24.78	19.14	0.06	0.03		12.0
SUS316L(A)	0.025	0.58	1.12	0.012	0.003	16.92	13.98	2.10			1.5
SUS316L(B)	0.021	0.57	1.15	0.033	0.002	17.40	12.67	2.03			1.5
SUS304L(A)	0.020	0.59	0.99	0.028	0.013	19.09	9.75	0.08			2.0
SUS304L(B)	0.017	0.51	1.48	0.025	0.005	18.50	9.73	0.05	0.03		12.0
SUS329J2L(A)	0.011	0.65	0.87	0.026	0.001	24.95	7.28	3.23	0.13	W:0.32	3.0
SUS329J2L(B)	0.017	0.57	1.75	0.028	0.001	22.13	5.49	2.92	0.14		12.0
SUS430(A)	0.060	0.33	0.70	0.028	0.008	15.92	0.09				2.0
SUS430(B)	0.070	0.64	0.57	0.027	0.005	16.24	0.48	0.05	0.01		12.0
SUS447J1	0.002	0.20		0.015	0.010	30.00		2.02	0.007		6.0

Table 2 Chemical compositions of deposited metals for SUS329J2L, duplex stainless steel

Mark	Chemical composition (wt.%)										Ferrite content*
	C	Si	Mn	P	S	Cr	Ni	Mo	O	N	(%)
1F	0.032	0.59	1.25	0.020	0.007	24.78	21.31	2.93	0.054	0.114	1
5F	0.029	0.57	1.19	0.020	0.007	24.26	15.42	2.70	0.056	0.102	6
20F	0.024	0.56	1.22	0.022	0.008	23.27	10.72	2.42	0.032	0.082	20
40F	0.032	0.57	1.18	0.020	0.010	24.76	9.62	2.82	0.056	0.119	44
60F	0.031	0.56	1.21	0.020	0.008	24.28	8.07	2.71	0.056	0.105	64
80F	0.031	0.65	0.96	0.026	0.006	24.26	4.75	2.94	0.019	0.107	77
99F	0.030	0.62	1.14	0.024	0.007	23.82	3.28	2.42	0.023	0.095	99

* Point count method

2.2 Experimental procedure

In order to get the clear solidification microstructure near the solidification front, liquid-tin quenching method[10] was used during GTA welding without filler metal. **Figure 1** shows the details of liquid-tin quenching apparatus. The quenching was done by dropping the specimen into the liquidized tin kept at 230°C, when the weld length was about 40mm. GTA welding conditions used are given in **Table 3**. For 1.5 to 6mm thick sheets, the welding current was changed with the constant welding speed of 50mm/min in order to get nearly the same weld heat input per unit thickness. The reason for the use of such slow welding speed is to make the formation of elongated columnar grains readily grow to the welding direction at the center of the bead. The welding conditions for 12mm thick plate was the same as that of the Trans-Varestraint test[5].

The solidification microstructure was observed mainly within the region corresponding to BTR (Brittleness Temperature Range) of the materials used. The BTR was quoted from the previous results which was obtained by the Trans-Varestraint test[5] and the tensile hot cracking

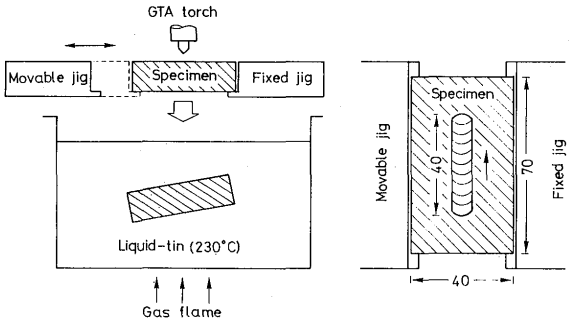

(a) Side view (b) Top view

Fig. 1 Schematic representation of liquid-tin quenching apparatus

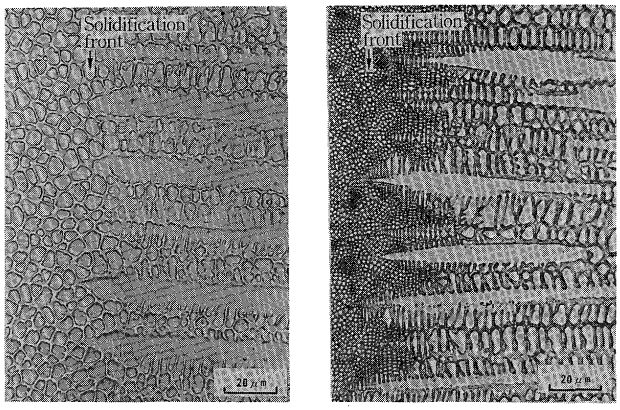

(a) Water quenching (b) Liquid-tin quenching

Fig. 2 Comparision of quenched solidification microstructures of SUS310S (12mmt)

Table 3 Welding conditions used

Thickness (mm)	Current (Amp)	Voltage (V)	Welding speed (mm/min)	Remarks
1.5	55	12	50	full penetration
2.0	70	12	50	
3.0	90	14	50	
6.0	180	18	50	nearly full penetration
12.0	250	19	150	same as Trans- Varestraint test

test[11] for the same materials used in this study. The surface temperature distribution along the center of the weld bead at just before quenching was estimated by the cooling rate measured with W-5%Re/W-26%Re thermocouple.

As etchant, 10% oxalic acid, 50% aquaregia or Kalling's reagent was used. When closer investigation was needed, SEM and EDX analysis were used.

3. Experimental Results and Discussion

3.1 Cooling effect of liquid-tin quenching

Figure 2 (a) and **(b)** compares the solidification microstructure near the solidification front of SUS310S obtained by water quenching and liquid-tin quenching, respectively. Cellular dendrites are observed evidently in both microstructures, but the microstructure quenched by liquid-tin clearly shows the secondary dendrite arms and their coarsening process just behind the solidification front. Moreover, the substructure which resulted from the quenching of molten puddle is extremely fine compared with that by water quenched microstructure.

In general, the secondary dendrite arm spacing is properer than the primary dendrite arm spacing for estimating the cooling rate during solidification[12]. Figure 2, however, shows no definite secondary dendrite arms in front of the solidification front, which was molten puddle. Therefore, the authors regardes the size of substructure in the molten puddle as primary dendrite arm spacing. Then, the correlation between cooling rate and primary dendrite arm spacing obtained by M.C. Flemmings[13] was extrapolated to get the cooling rate of liquidtin quenching. According to this estimation, the cooling rate at the moment of the liquid-tin quenching was about 1100°C/sec, compared with about 600°C/sec at the water quenching.

3.2 Solidification sequence of austenitic stainless steel

3.2.1 SUS310S

Figure 3 shows the quenched solidification microstructures of SUS310S within BTR. Cellular dendrites of the austenite can be seen evidently from the solidification front to the lower temperature limit of BTR, but no ferrite was observed at any temperature. With observing the microstructure closely, it is guessed that the solid bridge was formed around mark "A" near the solidification front due to the mutual contact of secondary dendrite arms growing from the neighbouring primary dendrite arms. Another characteristic of Fig. 3 is that the degree of etching of **(b)** 1330°C and **(c)** 1280°C is a little less than in **(a)** but nearly the same as that in (a). This

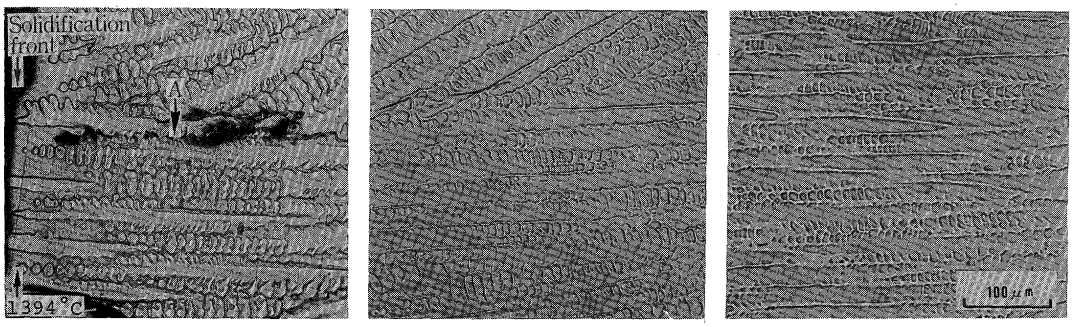

(a) Near solidification front (b) 1330°C (c) 1280°C

Fig. 3 Quenched solidification microstructures of SUS310S (12mmt). BTR ranged from 1394°C to 1276°C

means that the homogenization of microsegregation hardly occurs during cooling in the solid-liquid coexistent region, in contrast with SUS430 and SUS329J2L mentioned later.

A typical microstructure near the lower temperature limit of BTR is given in **Fig. 4**. Inclusions are observed at the location where the primary dendrite arm boundary intersects with the secondary dendrite arm boundary. This means that the residual liquid droplets are confined finally to this intersection due to the development of the solid bridge.

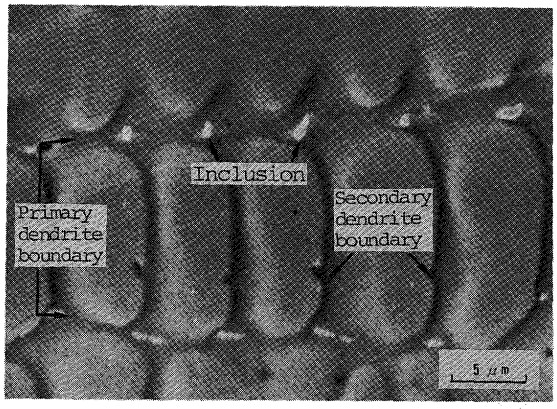

Fig. 4 Distribution of inclusions near the lower temperature limit of BTR of SUS310S (12mmt)

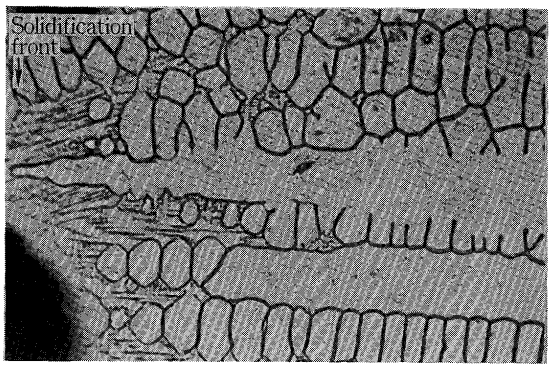

(a) 1430°C

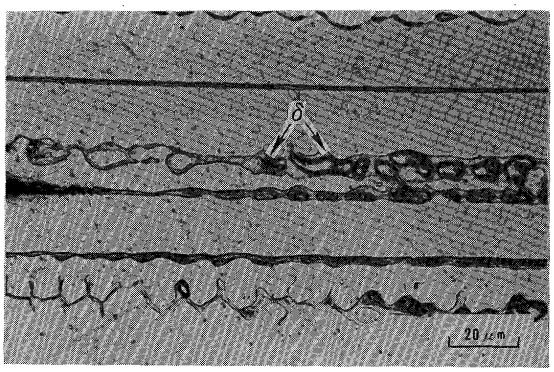

(b) 1400°C

Fig. 5 Quenched solidification microstructure of SUS316L(A) (1.5mmt)

3.2.2 SUS316L and SUS304L

In order to investigate the change of the solidification sequence with increasing the ferrite content, SUS316L and SUS304L were used. **Figure 5** shows the quenched solidification microstructures of SUS316L. Near the solidification front in **(a)**, only austenite solidifies dendritically and ferrite particles form at the interdendritic region of the austenite near 1400°C in **(b)** by the peritectic/eutectic reaction.

Figure 6 shows the quenched solidification microstructhre of SUS304L. As can be seen in **(a)**, primary solidifying phase is ferrite. Subsequently to the primary ferrite, the austenite of round shape started to be formed from about 1435°C and grew with decreasing the temperature. This austenite was formed at the cellular dendritic boundary of the ferrite as shown in (a). Moreover, it should be noticed that round inclusions in **(b)** enriched with P and S as shown in **(c)** were confined within the austenite grain. This means that the residual liquids enriched with P and S at the peritectic/eutectic temperature are enclosed by the austenite grain, and this directly confirms the model[14] shown in **(d)** which was proposed by the authors based on water-quenched microstructure and the material containing high S.

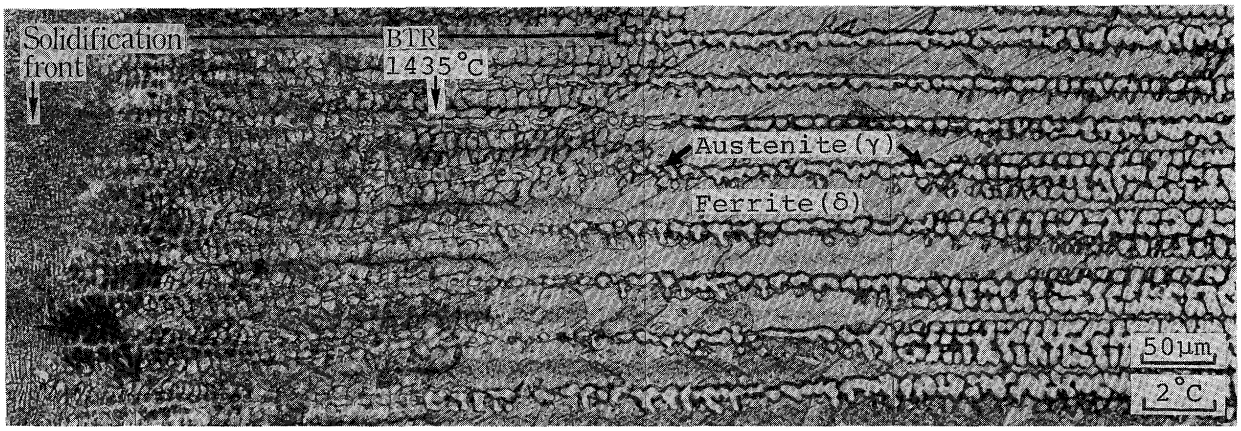

(a) Continuous solidification microstructure

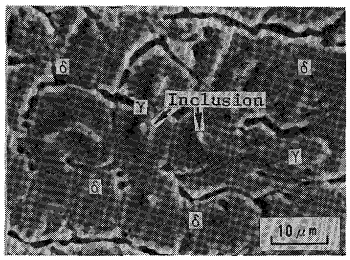

(b) Magnefied view near 1435°C in (a)

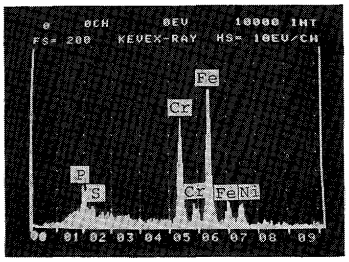

(c) EDX analysis of inclusion in (b)

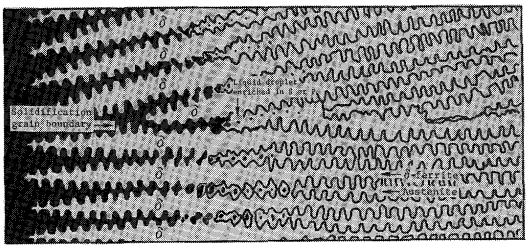

(d) Schematic illustration[14]

Fig. 6 Quenched solidification microstructure of SUS304L (2mmt)

3.3 Solidification sequence of ferritic stainless steel

The quenched solidification microstructure of SUS430 which solidifies with only ferrite is given in **Fig. 7**. Cellular dendrites are clearly observed near the solidification front. However, it was rapidly obscured during with decreasing the temperature and was barely visible at the lower temperature limit of BTR. In addition, it is interesting to note that the secondary dendrite arm boundary was rapidly obscured compared with the primary dendrite arm boundary. Also SUS447J1 showed nearly the same solidification sequence as SUS430. This characteristic feature means that the homogenization of microsegregation easily occurs during cooling in the solid-liquid coexistent region.

Another interesting feature of Fig. 7 is that the phase which is considered as austenite was seen at the interdendritic region near the lower temperature limit of BTR. However, it is not clear whether the austenite was formed during the solidification sequence or by rapid quenching during the solidification.

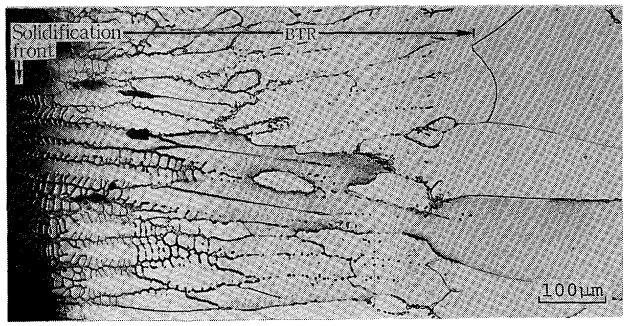

Fig. 7 Quenched solidification microstructure of SUS430 (2mmt)

3.4 Solidification sequence of duplex stainless steel

Figure 8 shows the quenched solidification microstructure of SUS329J2L. The solidification sequence is the same as the ferritic stainless steel, namely, cellular dendrites of the ferrite are drastically obscured with decreasing the temperature and no dendritic substructures are observed near the lower temperature limit of BTR. Moreover the secondary dendrite arm boundary was rapidly obscured compared with the primary dendrite arm boundary at the range of B to C as seen in Fig. 7. This means, the microsegregation caused by dendritic solidification was easily homogenized in the case of the secondary dendrite arm boundary.

Then, the actual formation temperature of the solid bridge was estimated from the following viewpoints: (i) the solid bridge is formed by the mutual contact of adjacent secondary dendrite arms growing from the neighbouring primary dendrite arms, (ii) the homogenization of microsegregation occurs by solid-state diffusion where the solid bridge is formed. With observing the microstructure

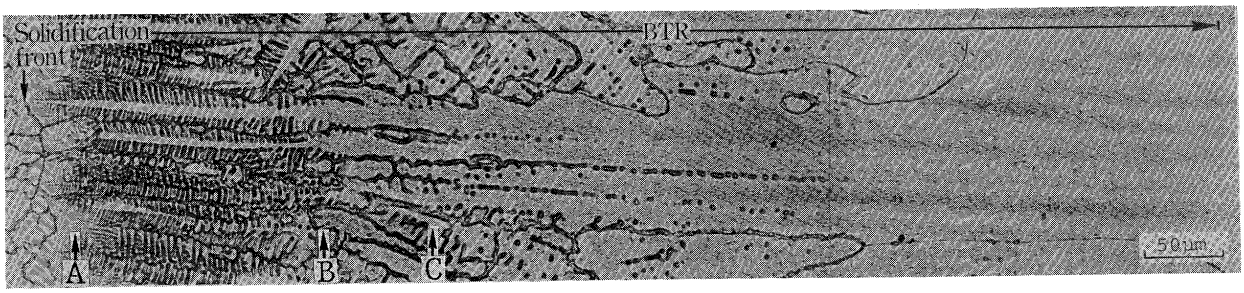

Fig. 8 Quenched solidification microstructure of SUS329J2L (12mmt)

closely, it is obvious that the above mentioned viewpoints of (i) and (ii) correspond to the location of A and the range of B to C in Fig. 8 respectively. These locations lied in about 5 to 20% of the BTR from the solidification front. As a result, it is judged that solid bridge was formed at very high temperature near the solidification front and was developed with decreasing the temperature. Due to the development of the solid bridge, the residual liquid was confined at the interdendritic boundary as liquid droplet shown in lower temperature region than C.

The weld metals which contain about 1% and 6% ferrite in the ambient temperature showed nearly the same solidification sequence as SUS310S and SUS304L respectively. However, the deposited metals which contain above 20% ferrite solidified with the primary ferrite. **Figure 9 (a)** and **(b)** show the quenched solidification microstructure of the deposited metals which contain 20% and 77% ferrite respectively. As can be seen in both microstructures, the solidification sequence is nearly the same as that of SUS430 and SUS329J2L. However, the needle-like Widmanstätten phase, which is considered as austenite, was seen near the lower temperature limit of BTR in (a). In addition, some of the grain boundary precipitation phase which is also considered as austenite, are visible at the solidification boundary. However, it is difficult to confirm whether the austenite was formed during the solidification sequence or by rapid quenching during the solidification.

4. Conclusion

Weld solidification sequence of the several kinds of stainless steels which have different solidification mode was observed by means of liquid-tin quenching method in order to reveal the cracking reason in the duplex austenitic-ferritic stainless steel.

Main conclusions obtained are as follows:

1) The cooling rate at the moment of liquid-tin quenching

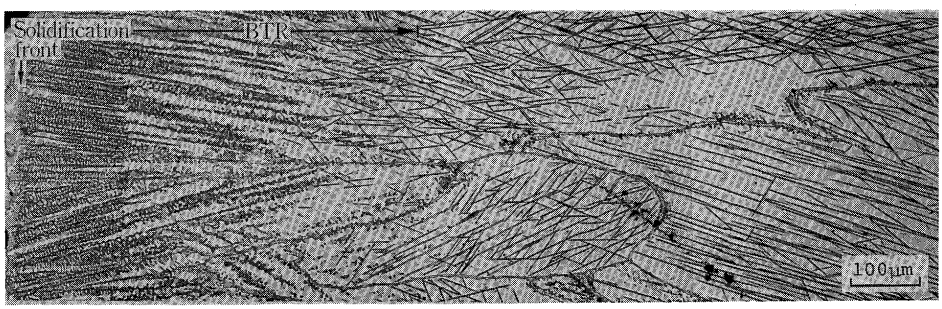

(a) Ferrite content: 20%

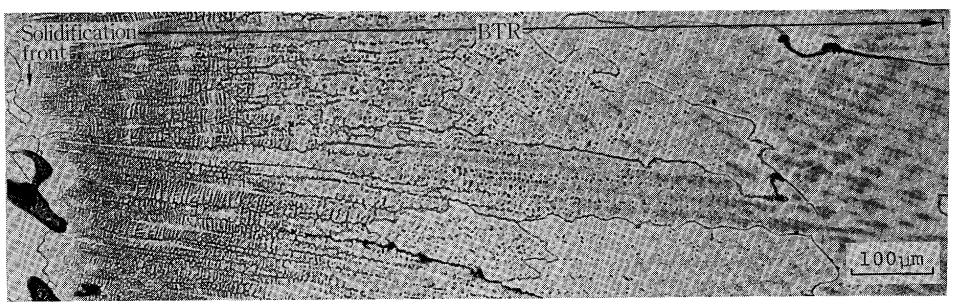

(b) Ferrite content: 77%

Fig. 9 Quenched solidification microstructure of deposited metals for SUS329J2L (12mmt)

was about 1100°C/sec. It has sufficient cooling rate to reveal the dendritic substructure even though weld metal which solidifies with primary ferrite.

2) The solidification sequence of the commercial stainless steels and several kinds of the deposited metals for SUS 329J2L, which contained 0 to 100% ferrite at the ambient temperature, was clearly observed by liquid-tin quenching method.
3) Solid bridge was formed at very high temperaure near the solidification front due to the mutual contact of adjacent secondary dendrite arms and it developed with decreasing the temperautre.
4) Due to the developing of the solid bridge, residual liquid droplets are confined to the intersectional site of the primary and the secondary dendrite arm boundary.
5) In the weld metal which solidifies with primary ferrite, cellular dendrites was rapidly obscured with decreasing the temperature even within the BTR. Moreover, the secondary dendrite arm boundary was apt to be obscured compared with the primary dendrite arm boundary. However, this feature was not noticeable in weld metal which solidifies with primary austenite.

Acknowledgement

The authors would like to thank Sumikin Welding Industries, Ltd. for the offering of a part of the materials used.

Reference

1) V. Kujanpää *et al.*: Welding Research International **9**, 2 (1979) p.55-76
2) V. Kujanpää *et al.*: Metal Const. **12**, 6 (1980) p.282-285
3) T.G. Gooch: Conf. Proc. Duplex Stainless Steels, ASM (1983) p.573-602
4) V. Kujanpää *et al.*: Metal Const. **17**, 1 (1985) p.40R-46R
5) F. Matsuda *et al.*: Trans. of JWRI **15**, 1 (1986) p.99-112
6) N.E. Nelson *et al.*: Welding Journal **66**, 8 (1987) p.241s-250s
7) T. Takalo *et al.*: Met. Trans. **10A**, 8 (1979) p.1173-1181
8) N. Suutala *et al.*: Met. Trans. **10A**, 8 (1979) p.1183-1190
9) N. Suutala *et al.*: Met. Trans. **11A**, 5 (1980) p.717-725
10) S. Kou *et al.*: Met. Trans. **13A**, 7 (1982) p.1141-1152
11) F. Matsuda *et al.*: Trans. of JWRI **12**, 1 (1983) p.73-80
12) T. Okamoto: Tetsu-to-Hagané **58**, 9 (1972) p.1302-1316 (in Japanese)
13) M.C. Flemmings *et al.*: JISI **208** (1970) p.371-381
14) F. Matsuda *et al.*: Trans. of JWRI **13**, 2 (1982) p.41-58